Anomalous backward scattering and quasimolecular structure of nuclei

K. A. Gridnev

A. A. Zhdanov Leningrad State University

A. A. Ogloblin

I. V. Kurchatov Institute of Atomic Energy, Moscow
Fiz. Élem. Chastits At. Yadra, 6, 393–434 (April–June 1975)

A currently important problem of nuclear physics is reviewed— large-angle scattering of complex particles such as α particles, ^{6}Li ions, etc. It is shown that backward scattering cannnot be described within the framework of traditional approaches such as the diffraction or the optical model. The various approaches used to explain anomalous backward scattering are discussed: glory scattering model, optical model with l-dependent imaginary part, reactions with exchange, Regge-pole method, repulsive-core method, etc. The connection between backward scattering and the cluster structure of nuclei is established.

PACS numbers: 25.70.

INTRODUCTION

Interest in the study of elastic scattering of nuclei on one another arose in the fifties, when the optical model of nucleon scattering was proposed and the natural attempt made to apply the concept and formalism of the optical model to the scattering of complex particles (deuterons, α particles, and more complicated nuclei).

It proved much harder to justify theoretically and actually implement in practice the description of scattering of complex particles by a potential than in the case of nucleon scattering. It is still not known to what extent the many-body problem (for example, scattering of two complex nuclei on one another) can be reduced to the motion of a point particle in a local and complex effective potential. The parameters of the potentials deduced by comparing experimental data with optical-model calculations are subject to numerous uncertainties, and this has prevented scattering data being used even for purely utilitarian purposes such as, for example, the description of a transfer reaction by the distorted-wave method.

The situation which existed until about 1969 can be briefly characterized as follows. The experimental data as a whole, especially for scattering on heavy nuclei, could be explained well under the assumption that there is strong absorption within the nucleus. The concept of strong absorption means that all partial waves with angular momentum less than a certain critical l_0 are absorbed by the nucleus and do not make a significant contribution to the scattering, while waves with $l > l_0$ are scattered and hardly absorbed at all. The limiting case of such an approach is the black-nucleus model with a sharp edge, in which the moduli of the S-matrix elements S_l are strictly zero for $l \leq l_0$ and unity for $l > l_0$. Better agreement with experiments is obtained by assuming that S_l varies smoothly from 0 to 1 in a narrow range of l.

In the language of the optical model, the concept of strong absorption means that the scattering is determined solely by the edge of the potential and is not sensitive to its interior behavior. Therefore, potentials that have different depths but the same "tail" give the same description of the scattering (in some cases, the depth of the real part of the potential varied from 20 to 1000 MeV). This explains the observed uncertainties of the potentials and, moreover, shows that in the case of strong absorption the interior part of the potential has no physical meaning. The values of S_l calculated by the optical model with strong absorption vary smoothly from 0 to 1 in a small range of l near a certain critical l_0, which is determined by the height of the barrier:

$$E = Z_1 Z_2 e^2/r + l_0(l_0+1)/(2\mu r^2). \quad (1)$$

If strong absorption is predominant in scattering, this process is of comparatively little interest for the study of nuclear structure. The investigations at the end of the fifties and in the sixties were aimed basically at elucidating the nature of the uncertainties in the potentials, developing methods of using these potentials to calculate reactions, and studying properties of the surface of the nucleus.

The fresh interest in scattering of complex particles developed after deviations from the concept of strong absorption had been found. Two experimentally ob-

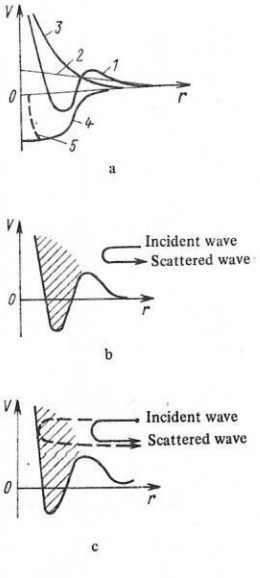

FIG. 1. Interaction potential of colliding nuclei: a) terms of the total interaction potential; b) case of strong absorption; c) case of weak absorption; the hatched region is the absorption region: 1) total interaction potential; 2) Coulomb potential $Z_1 Z_2 e^2/r$; 3) centrifugal potential $\hbar^2 l(l+1)/(2\mu r^2)$; 4) nuclear potential; 5) repulsive core.

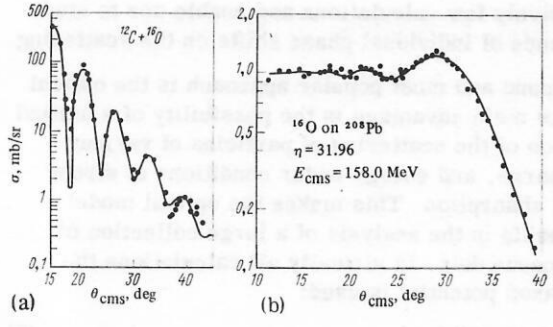

FIG. 2. Examples of Fraunhofer (a) and Fresnel (b) diffraction: • experiment; — optical model.

served effects—anomalously strong large-angle scattering and the structure of excitation functions—could not in principle be explained by the earlier conceptions. To describe these effects it was necessary to assume that partial waves with angular momenta near l_0 are absorbed much more weakly than is predicted by the older models. The transparency of the nucleus for surface partial waves results in interference between the waves (Fig. 1) reflected from the surface of the nucleus and the waves reflected from the inner part of the nucleus (centrifugal barrier or repulsive core). The interference of these waves is manifested by the S-matrix elements S_l ceasing to depend smoothly on l and becoming nonmonotonic, with bumps (see Fig. 5).

Because the surface partial waves are weakly absorbed, their orbiting becomes possible—an interaction between the two colliding nuclei in which they rotate about one another for a certain time without losing their individuality. In other words, a state rather like a nuclear molecule is formed. There is a classical analog which illustrates the orbiting effect. Take a small black sphere surrounded by a transparent shell and direct a beam of light on it. Under certain conditions, there can be total internal reflection of the transmitted light wave, which is trapped by the surface of the nucleus. The light is reflected from the shell and passes inward, being refracted. The weak absorption of the long waves in the surface layer of the nucleus and the formation of a standing wave in it strongly increase the backward scattering compared with the case of strong absorption. By varying the energy of the incident particles (wavelength), one can observe the orbiting of different successive waves, this being manifested by the appearance of resonances in the excitation curve.

The main interest in the study of the scattering of nuclei on one another is due to this possibility of obtaining and investigating molecule-like nuclear systems. One is particularly attracted by the possibility of studying the influence of the repulsive core, whose existence follows naturally from the Pauli principle for an interaction of quasimolecular type.

In this review, we shall consider only one aspect of the problem of the scattering of complex particles: intense large-angle scattering, which has been called anomalous because of the unexpectedly large cross section. We shall see that in many cases anomalous backward scattering is directly related to molecular

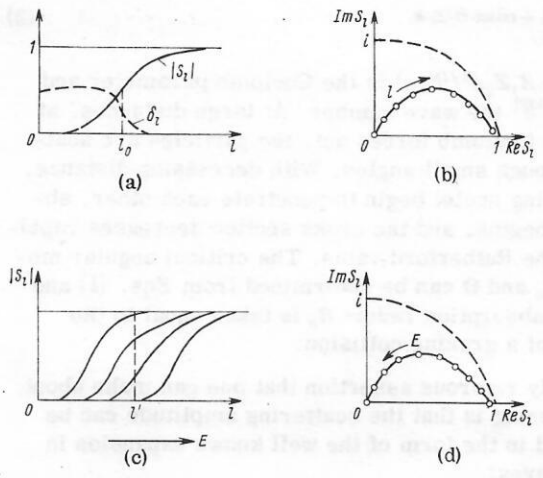

FIG. 3. Parametrization of the S-matrix elements and Argand diagrams: a) parametrization of $|S_l|$ and the phase shift δ_l by Fermi-type dependences; b) Argand diagram for fixed energy; c) values of $|S_l|$ for different energies; d) Argand diagram for fixed l.

effects of nuclear structure. In addition to the orbiting which we have already discussed, such scattering in the case of nuclei of comparable masses is sometimes due to the transfer of a cluster of particles from one nucleus to the other. As a result, anomalous backward scattering can be used to study cluster effects in the ground states of nuclei.

1. BASIC FEATURES OF ELASTIC SCATTERING

Let us review briefly the main features of elastic scattering of nuclei on one another and the methods used to describe it. In the classical description of scattering—usually a good approximation for heavy ions—the colliding nuclei move along paths and there is a unique relationship between the distance D of closest approach and the scattering angle Θ:

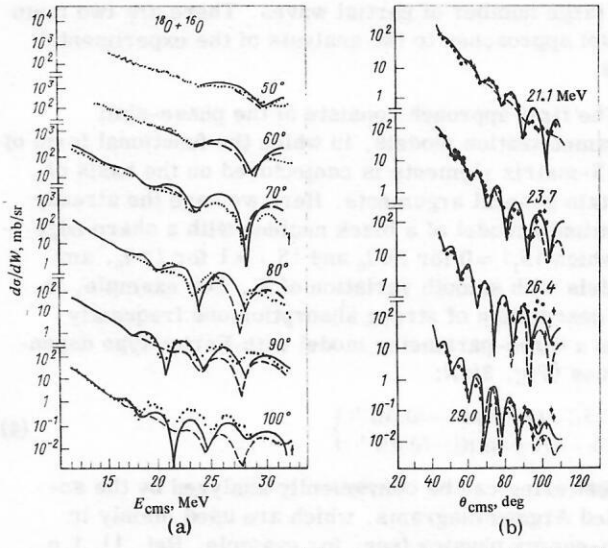

FIG. 4. Excitation functions (a) and angular distributions (b) of $^{18}O+^{16}O$ scattering: The continuous curves were calculated by the optical model with weak absorption; the dashed curves, with strong absorption. The parameters of the potentials are given in the text.

$$D = \eta\,(1 + \operatorname{cosec}\Theta/2)/k, \qquad (2)$$

where $\eta = Z_1 Z_2 e^2/(\hbar, v)$ is the Coulomb parameter and $k = \sqrt{2\mu E/\hbar^2}$ the wave number. At large distances, at which the Coulomb forces act, the particles are scattered through small angles. With decreasing distance, the colliding nuclei begin to penetrate each other, absorption begins, and the cross section decreases rapidly from the Rutherford value. The critical angular momentum l_0 and Θ can be determined from Eqs. (1) and (2) if the absorption radius R_0 is taken equal to the distance of a grazing collision.

The only rigorous assertion that one can make about the scattering is that the scattering amplitude can be expressed in the form of the well known expansion in partial waves:

$$f(\Theta) = f_c(\Theta) + \frac{i}{2k}\sum_{l=0}^{\infty}(2l+1)\exp(2i\sigma_l)\,(1 - S_l)\,P_l(\cos\Theta) \qquad (3)$$

(where $f_c(\Theta)$ and σ_l are the Coulomb amplitude and phase shift), which includes the elements of the S matrix:

$$S_l = A_l \exp(2i\sigma_l);\ A_l = |S_l| \leqslant 1.$$

Here, A_l is called the reflection coefficient. If there is no absorption, $A_l = 1$.

It is well known from the analysis of the experimental data that the form of the angular distributions is rather clearly determined by the relationship of η to kR (Fig. 2). At small η and large ($\gg 1$) kR the angular distributions have the character of Fraunhofer diffraction; for $\eta \approx kR \gg 1$, they have the character of Fresnel diffraction. At large η ($\gtrsim 6$) and small kR, the angular distributions are structureless and in a wide range of angles the cross section is a Rutherford one.

The elements of the scattering matrix S_l contain the entire information about the nuclear interaction. It is in practice impossible to carry out a phase-shift analysis in the case of scattering of heavy ions because of the large number of partial waves. There are two main model approaches to the analysis of the experimental data.

The first approach consists of the phase-shift parametrization models, in which the functional form of the S-matrix elements is conjectured on the basis of certain general arguments. Here we have the already mentioned model of a black nucleus with a sharp edge in which $|S_l| = 0$ for $l \leqslant l_0$ and $|S_l| = 1$ for $l > l_0$, and models with smooth variation of S_l. For example, in the description of strong absorption one frequently uses a three-parameter model with Fermi-type dependences (Fig. 3(a)):

$$\left.\begin{aligned} |S_l| &= \{1 + \exp[(l - l_0)/\Delta]\}^{-1}; \\ \delta_l &= \delta\{1 + \exp[(l - l_0)/\Delta]\}^{-1}. \end{aligned}\right\} \qquad (4)$$

Scattering can be conveniently analyzed by the so-called Argand diagrams, which are used mainly in high-energy physics (see, for example, Ref. 1), i.e., the plots of Im S_l against Re S_l, which behave normally and do not exhibit "loops" corresponding to resonances. The parametrization of resonances will be considered later. The phase-shift parametrization models require comparatively few calculations and enable one to study the influence of individual phase shifts on the scattering.

The second and most popular approach is the optical model. Its main advantage is the possibility of a unified description of the scattering of particles of various mass, charge, and energy under conditions of strong and weak absorption. This makes the optical model irreplaceable in the analysis of a large collection of heterogeneous data. In virtually all calculations the Woods-Saxon potential is used:

$$U = V_0 f_V(r) + iW_0 f_W(r) \qquad (5)$$

with radial dependence

$$\left.\begin{aligned} f_V(r) &= \{1 + \exp[(r - R)/a]\}^{-1}; \\ f_W(r) &= \{1 + \exp[(r - R)/a]\}^{-1};\ f'_W = \frac{d}{dr} f_W(r). \end{aligned}\right\} \qquad (6)$$

in which the radius R and the diffuseness a may be either the same or different for the real and the imaginary parts. The replacement of surface absorption by volume absorption for heavy ions does not make a significant difference.

As an example, we give the strong absorbing potential for heavy ions obtained in Ref. 2: $V = 100$ MeV, $W = 40$ MeV, $r_{0V} = r_{0W} = 1.20$ F, $a_V = 0.49$ F, $a_W = 0.32$ F. Potentials of this type give a good description of forward scattering but they are not capable of reproducing the angular distributions at large angles.

An example of a weakly absorbing potential is that of Maher *et al.*,[3] which was proposed for the description of the scattering of ^{16}O ions and has these parameters: $V = 17$ MeV, $W = 0.4 + 0.1\ E_{cms}$ MeV, $r_{0V} = r_{0W} = 1.35$ F, $a_V = a_W = 0.49$ F.

The excitation functions and angular distributions of $^{16}O + {}^{18}O$ scattering are given in Fig. 4. The experimental data are compared with calculations made with both these potentials. It can be seen that the weakly absorbing potential reproduces the observed structure much better. The discrepancy between the calculations based on the strongly absorbing potential and the experiment increases with increasing angle.

The S-matrix elements obtained from the calculation of the curves in Fig. 4 are given in Fig. 5. It can be seen that the reflection coefficients in the case of weak absorption exhibit nonmonotonicity, which we have already mentioned. The $|S_l|$ values for strong absorption are essentially averaged values compared with the foregoing case, and they smooth out the bumps.

We shall not here dwell on the numerous questions related to the use of the optical model, but turn directly to anomalous backward scattering.

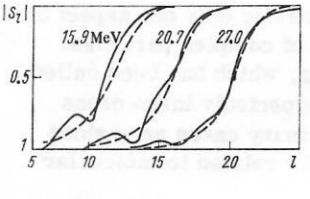

FIG. 5. Moduli of the S-matrix elements which describe the data of Fig. 4: the continuous curves correspond to weak absorption; the dashed, to strong absorption.

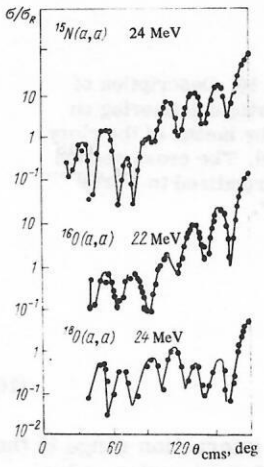

FIG. 6. Differential cross sections of α-particle elastic scattering on ^{15}N, ^{16,18}O nuclei.

2. ANOMALOUS BACKWARD SCATTERING (EXPERIMENTAL)

By anomalous backward scattering (ABS) one understands large and oscillating cross sections at angles from approximately 130 to 180°. The ABS sometimes exceeds Rutherford scattering by two or more orders of magnitude. This can be illustrated by the extensive material accumulated from the study of α-particle scattering on the nuclei ^{12}C, ^{14,15}N, ^{16,18}O, ^{24}Mg, ^{28}Si, ^{32}S, ^{36,38}Ar, ^{39}K, and ^{40,42,44,48}Ca at α-particle energies above the Coulomb barrier.[4] A typical angular distribution of α particles with energy 22–24 MeV scattered elastically on ^{15}N and ^{16,18}O nuclei is given in Fig. 6, which is taken from Ref. 5.

Anomalous backward scattering is manifested not only in the scattering of α particles but also for ^{6}Li, ^{12}C, ^{16,18}O, and ^{28}Si ions. Typical angular distributions of ^{6}Li ions scattered elastically on ^{4}He, ^{12}C, ^{16}O, ^{28}Si, and ^{40}Ca nuclei are shown in Fig. 7, which is taken from Ref. 6. It should be noted that ABS is generally observed most clearly for nuclei that have α-cluster nature: $4 \leq A \leq 48$. In this connection, the shell-filling effect of the target nuclei in ABS is interesting. There is now available extensive material on α-particle scattering on isotopes of carbon, nitrogen, oxygen, sulfur, argon, potassium, and calcium[4,5,7], and a number of general features can be established.

All nuclei between ^{9}Be and ^{48}Ca for which $N=Z$ and $N=Z+1$ exhibit ABS, which varies slowly with the energy of the incident particles. ABS is manifested in heavy isotopes if the same shell of the light isotope with $N=Z$ and $N=Z+1$ is filled; conversely, ABS is suppressed if two excess neutrons occupy the next shell outward. For example, ABS is observed in ^{36}Ar and also in ^{38}Ar (with two extra d neutrons) but is suppressed in ^{40}Ar (with two $f_{7/2}$ neutrons).

The ABS behavior in Ca isotopes as the $f_{7/2}$ shell is filled is interesting (Fig. 8). ABS is observed at the ends of the shell in ^{40}Ca and ^{48}Ca but is suppressed in ^{42,44}Ca. This suppression can be explained by the coupling of the neutrons to the levels of a rotational band.

Optical-model calculations by Gaul[4] showed that no average optical potential could describe the scattering

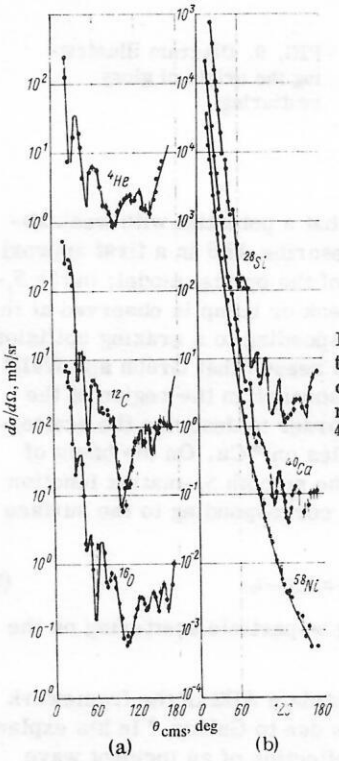

FIG. 7. Differential cross sections of the elastic scattering of ^{6}Li ions on the following nuclei: a) ^{4}He, ^{12}C, ^{16}O; b) ^{28}Si, ^{40}Ca, ^{58}Ni.

on neighboring nuclei and isotopes. It is necessary to make additional assumptions about the reaction mechanism. Below, we describe the existing ways in which ABS is explained.

3. SIMPLEST EXPLANATIONS OF ANOMALOUS BACKWARD SCATTERING

All the simplest ways of explaining ABS are related in some way or another to the influence of the angular momentum corresponding to a grazing collision. We

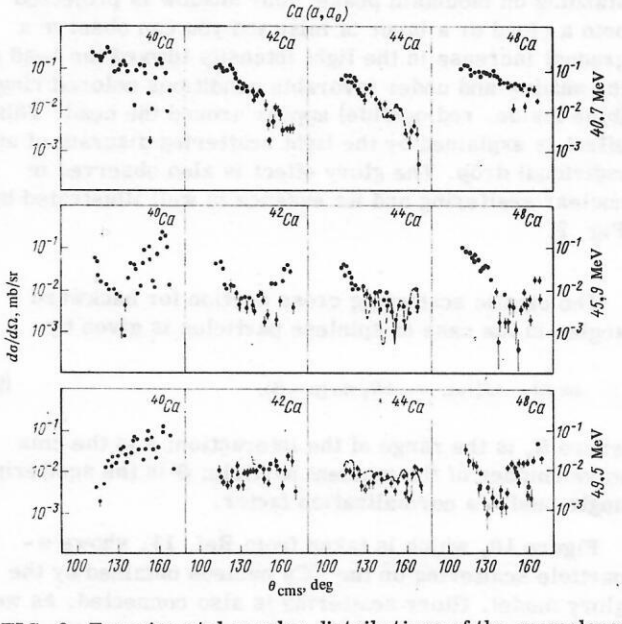

FIG. 8. Experimental angular distributions of the anomalous backward scattering of α particles on Ca isotopes at different energies.

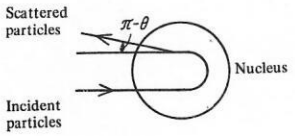

FIG. 9. Diagram illustrating the origin of glory scattering.

have already pointed out that a potential with weak absorption enables one to describe ABS in a first approximation in the framework of the optical model; in the S_l-matrix moduli, a small peak or bump is observed at the angular momentum corresponding to a grazing collision (see Fig. 5). It is for this reason that Gruhn and Wall[8] assume that there is a resonance in the region of the surface of the nucleus in order to describe the scattering of 30.5-MeV α particles on ^{40}Ca. On the basis of this, they make a dip in the smooth S_l-matrix function at the angular momentum corresponding to the surface of the nucleus, $l_s \sim ka$:

$$S_l = \{1 + \exp[(l - l_0)/\Delta]^{-1} - \mu_s \delta (l - l_0) \tag{7}$$

and succeed in describing α-particle scattering on the ^{40}Ca nucleus.

A different attempt to explain ABS in the framework of the diffraction model is due to Gubkin.[9] In his explanation, ABS is due to the reflection of an incident wave on the surface of the nucleus due to the abrupt change of the wavelength on the transition from the exterior to the interior region of the nucleus. Allowance for reflection leads to the following parametrization of the S_l matrix:

$$S_l = \eta_l + C \exp(i\pi l)[1 - \eta_l]. \tag{8}$$

The factor $\exp(i\pi l)$ enhances the flux in the direction π.

On the basis of optical analogies, Ford and Wheeler[10] and also Bryant and Jarmie[11] show that scattering into the region 140–180° can be regarded as glory scattering. In optics, the term "glory" was first introduced by Van de Hulst.[12] This phenomenon can be observed by standing on mountain peaks: your shadow is projected onto a cloud or a layer of mist and you can observe a gradual increase in the light intensity toward the head of the shadow and under favorable conditions colored rings (blue inside, red outside) appear around the head. This effect is explained by the light scattering diagram of an individual drop. The glory effect is also observed in nuclear scattering and its essence is well illustrated by Fig 9.

The elastic scattering cross section for backward angles in the case of spinless particles is given by

$$d\sigma/d\Omega = AJ_0^2(u); \quad u = kR_g \sin(\pi - \Theta), \tag{9}$$

where R_g is the range of the interaction; k is the cms wave number of the incident particle; Θ is the scattering angle; and A a normalization factor.

Figure 10, which is taken from Ref. 11, shows α-particle scattering on the ^{40}Ca nucleus obtained by the glory model. Glory scattering is also connected, as we mentioned at the start, with the angular momentum corresponding to a grazing collision. This can be seen very well from the relation

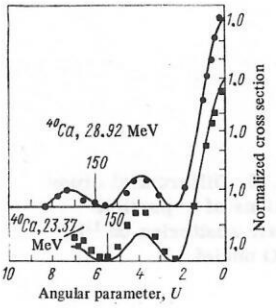

FIG. 10. Description of α-particle scattering on ^{40}Ca by means of the glory model. The cross section is normalized to 1 at $\Theta = 180°$.

$$\lim_{l \to \infty} P_l(\cos\Theta) = J_0(l\Theta). \tag{10}$$

It is interesting to note that the interaction range in the glory model in the region of backward angles is less than in the case of fitting to the forward angles in accordance with the diffraction formula. This fact was first noted by Bobrowska *et al.*[13] In a different paper,[14] the same experiment of Ref. 13 was analyzed by means of the optical model. It was shown that fitting by the optical model is possible if the forward and backward angles are fitted separately.

In some cases[15] of backward scattering of α particles, resonances are observed in the excitation functions. A resonance can be explained most easily by introducing a Breit-Wigner term into the scattering amplitude in the form

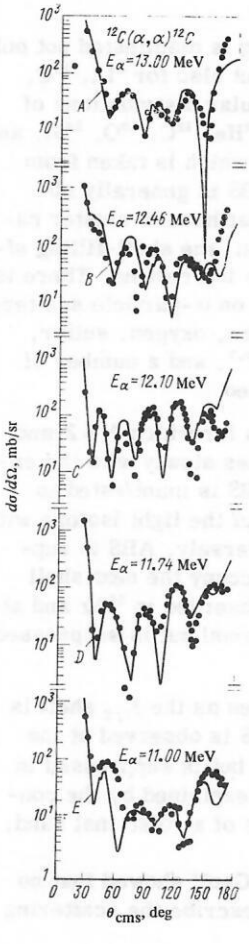

FIG. 11. Angular distributions and fits with several resonant phase shifts in accordance with the absorbing model of elastic scattering of α particles on ^{12}C at different energies.

$$S_l = \exp(2i\eta_l)\left[1 - i\sum_R \frac{\Gamma_0}{E - E_R + i\Gamma/2}\right]. \quad (11)$$

Carter *et al.*[16] use an absorbing model with resonant phase shifts to interpret α-particle scattering in the energy range 11–19 MeV on ^{12}C nuclei. The experimental angular distributions and a fit with some resonance terms for the $^{12}C(\alpha,\alpha)^{12}C$ reaction are given in Fig. 11. It can be seen that the calculations agree satisfactorily with the experiment. ABS can be described in this way when resonances can be traced in the excitation functions. However, it must be emphasized that ABS is also observed when resonances are not. Examples of this will be discussed below.

4. EXCHANGE OF CLUSTERS BETWEEN TWO IDENTICAL CORES

The simplest interactions in atomic physics are those in which an electron is exchanged between a proton and a hydrogen atom. The exchange of nucleons between two nuclear cores was first considered by Temmer.[17] On the basis of the general principles of quantum mechanics, one can show that in the scattering $A^I(B,B)A^I$ there is a large contribution from the exchange transfer $A^I(B,A)B^I$ if the nucleus B has a large reduced width[18] against breakup: $B = A + C$. Figure 12 shows clearly the difference between the elastic scattering $A^I(B,B)A^I$ and the exchange transfer reaction $A^I(B,A)B^I$.

At distances at which the wave functions overlap, the exchange interaction as a function of the distance between the cores is given by the exchange integral $J(\mathbf{R})$ (see Fig. 12 for the notation):

$$J(\mathbf{R}) = \int \Phi_{B^I}(\mathbf{r}_{AC})\, V_{B^I}(\mathbf{r}_{AC})\, \Phi_{B^I}(\mathbf{r}_{AI_B})\, d\mathbf{r}_{AC}, \quad (12)$$

where $\mathbf{R} > \mathbf{r}_{AI_C}$, $\mathbf{r}_{AC}$; $\mathbf{r}_{AC} = \mathbf{r}_{AI_C} - \mathbf{R}$. At large distances $\mathbf{R}$ between the cores, the interaction has a radial dependence of the form $\exp(-\alpha R)/\alpha R$, where $\alpha = \sqrt{2\mu_C E_B/\hbar^2}$ and E_B is the energy of binding of particle C to the core.

Introducing the scattering amplitudes $f_I(\Theta)$ and $f_{II}(\Theta)$, which are obtained by adding (I) or subtracting (II) the interaction $J(\mathbf{R})$ relative to the optical potential, the differential cross section of elastic scattering, σ_{BB}, and of the exchange process, σ_{BA}, become

$$\left.\begin{aligned}\sigma_{BB}(\Theta_B) &= |[f_I(\Theta_B) + f_{II}(\Theta_B)]/2|^2;\\ \sigma_{BA}(\Theta_A) &= \sigma_{BB'}(\pi - \Theta_B') = |[f_I(\Theta_A) - f_{II}(\Theta_A)]/2|^2.\end{aligned}\right\} \quad (13)$$

The differential cross section of the exchange process, σ_{BA}, gives a rise of the differential cross section at backward angles. If $J(\mathbf{R}) = 0$, then $f_I(\Theta) = f_{II}(\Theta)$, and σ_{BB} is the ordinary elastic-scattering cross section; $\sigma_{BA} = 0$.

In the reaction $A^I(B,A)B^I$ it is in principle impossible to decide whether the outgoing particle results from the elastic scattering $A^I(B,B)A^I$ or the transfer process. The angles of departure of the two processes can be expressed in terms of one another: $\Theta_{B'} = \pi - \Theta_A$, and their amplitudes must add. In order to understand the exchange process better, let us consider, following Von Oertzen,[18] the semiclassical treatment of the scattering process in the case of perfect localization of wave packets. We shall consider the exchange process in time, i.e., a nonstationary process. In this case, the superposition of the states (I) and (II) with their wave functions $\Psi_I(\mathbf{R}) = (\varphi_B + \varphi_{BI})/\sqrt{2}$, and $\Psi_{II}(\mathbf{R}) = (\varphi_B - \varphi_{BI})/\sqrt{2}$ can be represented by the equation

$$\begin{aligned}\Phi(t) = A\Big\{&\Psi_I \exp\Big[-i\int_{-\infty}^{t}\frac{J(\mathbf{R})}{\hbar}dt\Big]\\ &- \Psi_{II}\exp\Big[-i\int_{-\infty}^{t}\frac{J(\mathbf{R})}{\hbar}dt\Big]\Big\} = \varphi_{BI}\cos\Big[\int_{-\infty}^{t}\frac{J(\mathbf{R})}{\hbar}dt\Big]\\ &+ i\varphi_B\sin\Big[\int_{-\infty}^{t}\frac{J(\mathbf{R})}{\hbar}dt\Big] = \varphi_{BI}C_1(t) + i\varphi_B C_2(t).\end{aligned} \quad (14)$$

We are interested in the situations as $t \to +\infty$, i.e., after the collision. The integral with respect to the time of the exchange interaction is the action function $S = \int_{-\infty}^{\infty} J(\mathbf{R}(t))\,dt$. The probabilities of finding particle C together with the core A or A^I are given, respectively, by the squares of the moduli of the coefficients C_1 and C_2:

$$|C_1(t)|^2_{t\to\infty} = \cos^2[S/\hbar]; \quad |C_2(t)|^2_{t\to\infty} = \sin^2[S/\hbar].$$

This can be best represented by an idealized picture which characterizes the exchange process with a changing distance between the cores in time and is shown in Fig. 13.

In the treatment of the exchange process it has been assumed that the spins of the cores are zero and that particle C is exchanged with angular momentum $l = 0$ near the Coulomb barrier. Essentially, Von Oertzen's method is the method of linear combination of nuclear orbitals, which corresponds completely to the method of linear combination of atomic orbitals in atomic physics.[19]

The total wave function in the method of molecular functions is

$$\Psi^+(\mathbf{R}, \mathbf{r}_c) = \sum_p \chi_p(\mathbf{R})\,\Psi_p(\mathbf{R}, \mathbf{r}_c), \quad (15)$$

where $\chi_p(\mathbf{R})$ is the wave function of the relative motion of the cores; $\Psi_p(\mathbf{R}, \mathbf{r}_c)$ is the wave function of the valence particle C, which depends on the distance $\mathbf{R}$ between the cores. The wave function of the valence particle in the method of linear combination of nuclear orbitals is ex-

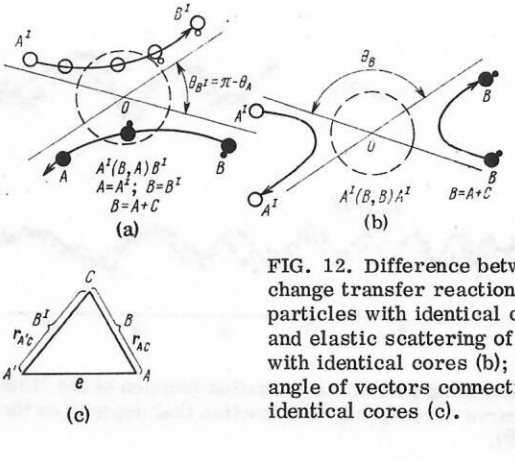

FIG. 12. Difference between exchange transfer reaction between particles with identical cores (a) and elastic scattering of particles with identical cores (b); the triangle of vectors connecting the identical cores (c).

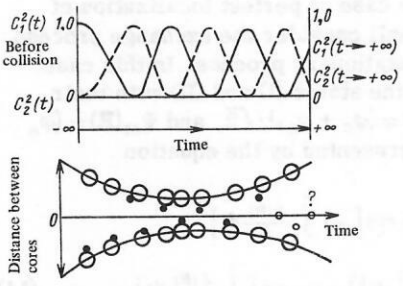

FIG. 13. Exchange process with varying distance between the cores in time.

pressed in terms of the nuclear orbitals $\Psi_{lm}(\mathbf{r}_{AC})$ and $\Psi_{l'm'}(\mathbf{r}_{A'C})$ of this particle:

$$\Psi_p^{\lambda J}(\mathbf{R}, \mathbf{r}_C) = N(R)\,[\varphi_{lm}(\mathbf{r}_{AC}) \pm \varphi_{l'm'}(\mathbf{r}_{A'C})]/\sqrt{2}. \tag{16}$$

The subscript p distinguishes even and odd functions; λ is the projection of the angular momentum J onto the molecular axis.

For even and odd wave functions, there is a system of decoupled equations:

$$\left(-\frac{\hbar^2}{2\mu}\nabla_R^2 + U_{AA'}(\mathbf{R}) + \langle\Psi_p^{\lambda J}|H|\Psi_p^{\lambda J}\rangle\right)\chi_p^{\lambda J}(\mathbf{R}) = 0, \tag{17}$$

where H is the Hamiltonian of the molecular system; $U_{AA'}(\mathbf{R})$ is the core-core potential, which is usually taken from the optical model; the matrix element $\langle\Psi_p^{\lambda J}|H|\Psi_p^{\lambda J'}\rangle = J^{\lambda J}(\mathbf{R})$ is the exchange interaction. As Baur and Gelbke[20] show, the distorted-wave method and the method of linear combination of nuclear orbitals give the same results.

Thus, we assume that the main contribution to the scattering at backward angles is made by exchange reactions. In this case, the elastic-scattering cross section will be determined by the expression

$$\begin{aligned}\sigma(\Theta, E) &\approx |f_g(E, \pi-\Theta) - f_u(E, \pi-\Theta)|^2 \\ &= |f_u|^2 + |f_g|^2 - 2|f_u||f_g|\cos(\beta_u - \beta_g) \\ &= |f_u - f_g|^2 + 4|f_u||f_g|\cos^2(\alpha/2 + \pi/4); \quad \alpha = \beta_u - \beta_g,\end{aligned} \tag{18}$$

where f_u and f_g are the scattering amplitudes corresponding to antisymmetric and symmetric wave functions, respectively.

If it is assumed that $f_u \sim f_g$, then, in accordance with (18), the oscillating part of the cross section must, depending on the energy and the assumption of independence of the collision parameter, be proportional to $\cos^2(\alpha/2 + \pi/4)$, where $\alpha/2 = \Delta E \Delta R/(\pi v)$. The oscillating part of the cross section has the same form as in the Landau-Zener-Stueckelberg formula, which describes the probability of transition to the inelastic channel in the case of atomic collisions.[21] Such oscillations of the excitation function have been observed by Kelleter *et al.*[22] who investigated the scattering of α particles on ^{7}Li nuclei in the energy ranges 8.6—12.5 and 17—22.5 MeV at the angles 54.2, 72.4, and 89.8°.

The oscillating part of the excitation function is shown in Fig. 14. It should be noted that such oscillations in the excitation functions were observed much earlier in atomic collisions in charge-exchange processes (in our terminology, this is elastic transfer), for example, in the reaction $Na^+ + Ne \to Na + Ne^+$.[23] The order of magnitude of $\Delta E \Delta R$ deduced from experiment is the same as in the case of nuclear collisions, i.e., approximately $3 \cdot 10^{-7}$ eV-cm.

If we take the parallel between atomic and nuclear collisions further, we must consider inelastic scattering channels. In inelastic channels in the case of atomic collisions an oscillating structure has been observed in the total cross sections,[24] for example, in the process $Na^+ + Ne \to Na^+ + Ne^+ \to \lambda 735.9$ Å (Fig. 15). This structure was interpreted as the interference of quasimolecular terms with neighboring energies. In the inelastic

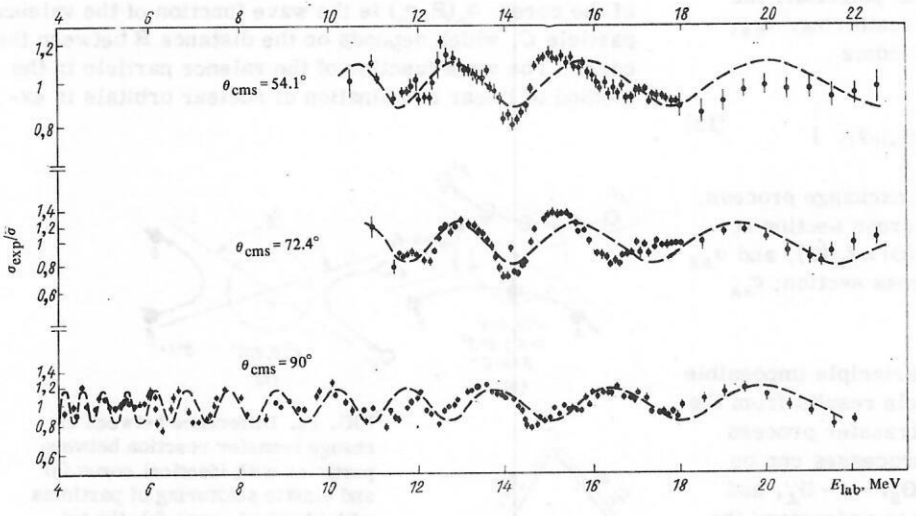

FIG. 14. Oscillating part of the excitation function of the ^{7}Li(α,α)^{7}Li reaction: the dashed curve corresponds to a function that depends on the time $1 + \beta\cos(2a/\sqrt{E})$.

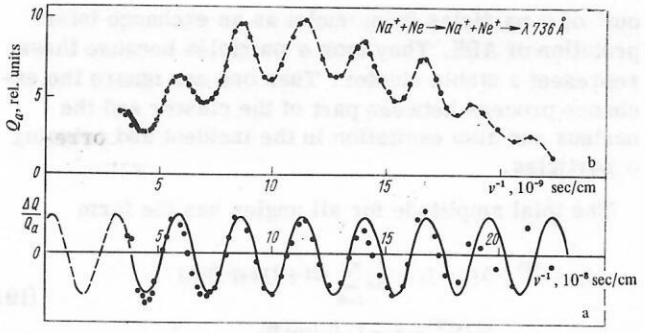

FIG. 15. Time dependence of the total cross section Q_a and the oscillating part $\Delta Q/Q_c$ of the cross section (Q_c) of the interaction of Na^+ ions with Ne atoms.

collisions of nuclear particles an oscillating structure has also been observed, for example, in Ref. 5, in the excitation functions. It is evident that here too there is interference between quasimolecular states. It is not fortuitous that we here direct attention to the study of excitation functions in exchange processes, since we believe that such a direction is promising.

A classical example that demonstrates the role of exchange processes in elastic scattering is the elastic scattering of oxygen ions on ^{12}C nuclei.[18] The elastic scattering of ^{16}O ions on ^{12}C nuclei at 35 MeV is shown in Fig. 16. The contribution of exchange processes was calculated by the distorted-wave method. It can be seen that the backward angles are explained by the competing α transfer $^{12}C(^{16}O, ^{12}C)^{16}O$, which is related to the elastic scattering by the relation $\theta_{cms}(^{12}C) = \pi - \theta_{cms}(^{16}O)$. The large cross section of the transfer process at backward angles is explained by the fact that the initial and final configurations are identical.

It is particularly interesting to investigate exchange in the simplest system in which cluster exchange is possible—scattering of deuterons and α particles on ^6Li nuclei. It has now been established with reasonable certainty that ^6Li has a cluster structure of the type $\alpha + d$, and this is manifested in different nuclear interactions of ^6Li (see, for example, Ref. 25). Therefore, in the scattering of α particles and deuterons through large angles strong backward scattering must arise.

The $^6Li + d$ and $^6Li + \alpha$ differential scattering cross sections taken from Ref. 26 are given in Fig. 17. It can be seen that the cross section does indeed increase strongly at large angles. The backward peak can also be very clearly observed in the $^6Li + \alpha$ scattering at about 150 MeV.[27] The large-angle cross sections cannot be reproduced by the optical model but can be fairly simply obtained under the assumption of exchange.

It is of great interest to consider how $^3He + ^6Li$ scattering will behave at large angles. Calculations made in the framework of nucleon-cluster models suggest[28] that in ^6Li not only the $\alpha + d$ configuration but also the cluster configuration $^3He + T$ is present; then the ratio of the spectroscopic factors (for an α-particle and deuteron separation parameter $x = 0.4$) is found to be $S(^3He + T)/S(\alpha + d) \approx 0.5$. According to the ordinary ideas, a strong backward peak should be observed in $^6Li + ^3He$ scattering.

The experiment of Ref. 26 shows that this is not so. Figure 17 gives the $^6Li + ^3He$ differential scattering cross section at a cms energy near the $^6Li + \alpha$ case (22.7 MeV and 21.9 MeV, respectively). The cross sections of the two processes in the forward hemisphere have very similar magnitudes, and the angular distribution curves almost coincide. But in the backward hemisphere the differences are very great—in one case there is anomalous backward scattering and, therefore, exchange; in the other there is not.

Thus, the clusters predicted by the cluster model are not manifested in the backward scattering. Nor are they manifested in the triton transfer reaction (^6Li, ^3He) in the case of excitation of certain states which are copiously formed in the "real" triton transfer reaction

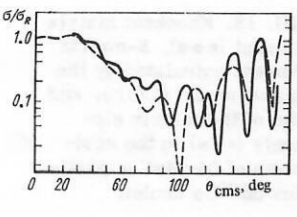

FIG. 16. Elastic scattering of ^{16}O ions on ^{12}C nuclei at 35 MeV: the continuous curve is the experimental one; the dashed curve is calculated by the optical model with allowance for the exchange interaction.

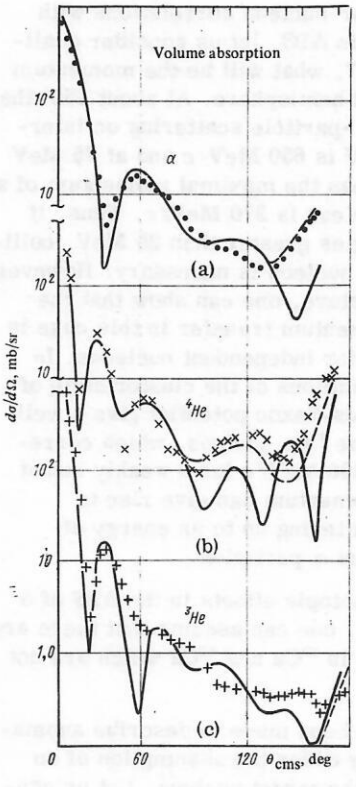

FIG. 17. Angular distributions of the elastic scattering of 36.6-MeV α particles, 34-MeV ^3He ions, and 19.6-MeV deuterons on ^6Li nuclei: The continuous curves are calculated in accordance with the optical model with volume absorption; a) α particle with parameters $V = 170$ MeV, $W = 12$ MeV, $r_{0V} = 1.15$ F, $r_{0W} = 1.7$ F, $a_V = 0.65$ F, $a_W = 1.15$ F; b) ^3He ions with $V = 100$ MeV, $W = 16.5$ MeV, $r_{0V} = 1.15$ F, $r_{0W} = 1.7$ F, $a_V = 0.63$ F, $a_W = 0.94$ F; c) deuterons with $V = 75$ MeV, $W = 11.6$ MeV, $r_{0V} = 1.15$ F, $r_{0W} = 1.7$ F, $a_V = 0.76$ F, $a_W = 1.0$ F; the dashed curve is the result of calculating the exchange process by the distorted-wave method.

(^{7}Li,α). On the other hand, the quasielastic knockout ^{6}Li(p,p^3 He)T behaves like scattering on the cluster ^{3}He in ^{6}Li.

Evidently, we are here concerned with the question of the extent to which the clusters in the nucleus are spatially separated. It is obviously difficult for the interpenetrating clusters within a nucleus predicted by the cluster model to be manifested in surface processes such as transfer reactions (or exchange scattering). This is reflected by the fact that the reduced width which characterizes the probability of a given subsystem being manifested at the radius of the channel can be small despite a large spectroscopic factor, which corresponds to integration over the whole volume of the nucleus. With increasing energy, exchange may still become observable, since deeper regions of the ^{6}Li nucleus become accessible. Therefore, the study of ^{6}Li + ^{3}He scattering at high energies is of great interest.

Thus, study of the exchange process in anomalous backward scattering may be a tool for investigating different types of clusters in nuclei.

5. ANOMALOUS BACKWARD SCATTERING ON SUBSTRUCTURES

To understand how four-nucleon correlations with $T=0$ can be manifested in ABS, let us consider qualitatively, following Ref. 7, what will be the momentum transfer in the backward hemisphere. At about 150° the momentum transfer in α-particle scattering on intermediate nuclei at 25 MeV is 650 MeV/c and at 75 MeV it is 1150 MeV/c, whereas the maximal momentum of a nucleon in the target nucleus is 270 MeV/c. Thus, if ABS is to occur at energies greater than 25 MeV, collision with more than one nucleon is necessary. However, assuming a quartet structure, one can show that the maximally possible momentum transfer in this case is four times greater than for independent nucleons. In particular, simple calculations of the cluster state of an α particle in the Woods-Saxon potential give a well depth of ~140 MeV for the ^{40}Ca nucleus, which corresponds to a momentum 900 MeV/c for a weakly bound cluster state. Such a momentum can give rise to anomalous backward scattering up to an energy of ~100 MeV for the incident α particles.

Bearing in mind the isotopic effects in the ABS of α particles on Ca isotopes, one can assume that there are inert groups of nucleons in ^{40}Ca and ^{48}Ca which are not present in ^{44}Ca.

Several attempts have been made to describe anomalous backward scattering under the assumption of an α-particle structure of the target nucleus. Let us consider the first attempt to explain ABS: calculation of the knockout amplitude by the distorted-wave method with allowance for antisymmetrization.[29] Agassi and Wall[29] were led to include the knockout amplitude in the elastic cross section by the following consideration: If a cluster exists, it must be on the surface of the nucleus, and the knockout amplitude Δf_N has a peak in coordinate space in the neighborhood of the nuclear radius $l_0 \sim kR$ and is small in magnitude. Agassi and Wall regarded "knockout" of α particles from nuclei as an exchange interpretation of ABS. They took α particles because these represent a stable cluster. Then one can ignore the exchange process between part of the cluster and the nucleus and also excitation in the incident and outgoing α particles.

The total amplitude for all angles has the form

$$f_N = f_N^{\text{opt}} + \Delta f_N = f_c + \frac{1}{2ik}\sum_{l=0}^{\infty}(2l+1)\exp(2i\sigma_l) \times (S_l^{\text{opt}} + a_l - 1)\,P_l(\cos\Theta). \tag{19}$$

The antisymmetrized T-matrix element for the reaction $a+\alpha \to b+\beta$ is given in accordance with the distorted-wave method by

$$T_{\alpha\beta} = \sum_p (-1)^p \langle \Psi_b \Psi_\beta \chi^{(-)}(\mathbf{r}_\beta \mathbf{k}_\beta) N_\beta - u_\beta P \Psi_a \Psi_\alpha \chi^{(+)}(\mathbf{r}_\alpha \mathbf{k}_\alpha)\rangle, \tag{20}$$

where p is the operator of permutation between the coordinates of the functions Ψ_α and Ψ_a; $(-1)^p$ ensures a plus sign if an even number of particles is exchanged and a minus sign if an odd number is. After a number of manipulations, one can obtain the correction a_l due to the knockout process:

$$a_l = \frac{-4iM}{\hbar^2 k}\sum_{nL\lambda}\frac{1}{c}\langle \Psi_\alpha | A_{nL}^{+}(\alpha) A_{nL}(\alpha) | \Psi_\alpha\rangle \begin{pmatrix} l & \lambda & L \\ 0 & 0 & 0 \end{pmatrix}^2 I(l,\lambda,L). \tag{21}$$

The matrix element $\langle \Psi_\alpha | A_{nL}^{+}(\alpha) A_{nL}(\alpha) | \Psi_\alpha\rangle$ is a measure of the number of α particles in the total antisymmetrized wave function Ψ_α; the operator A_{nl}^{+} is the α-particle creation operator;

$$I(l,\lambda,L) = \int dR_1\, dR_2 f_l(k,R_1)\Phi_{nL}(R_2) V_\lambda(R_1 R_2)\Phi_{nL}(R_1) f_l(R_2,k);$$

$C=(4!)^2$ for one species of particle; $C=(2!)^4$ for two species.

The quantum numbers of an α particle in an harmonic-oscillator potential satisfy the relation

$$2(n-1)+L = \sum_{i=1}^{4}[2(n_i-1)+l_i]. \tag{22}$$

Agassi and Wall show that the expression (21) has a peak in l, and also that ABS must disappear with increasing energy. As an illustration, they consider scattering of 24-MeV α particles on ^{40}Ca nuclei. The anomalous backward scattering is explained satisfactorily. Figure 18 shows the S-matrix element and the correction a_l to it. It can be seen that the correction has a peak in the region of the transition angular momenta l.

Another microscopic approach to the explanation of ABS is to calculate the heavy-particle stripping amplitude. Noble and Coelho[30] show that heavy-particle stripping is in principle capable of explaining α-particle backward scattering on ^{16}O nuclei with allowance for the

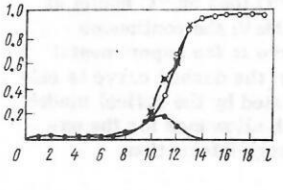

FIG. 18. Knockout matrix element (●●●), S-matrix element calculated by the optical model (○○○), and sum of the matrix elements (×××) in the scattering of 24-MeV α particles on ^{40}Ca nuclei.

cluster structure of ^{16}O and ^{12}C. However, it is not clear how accurate are the approximations they make.

Finally, a third approach to the explanation of ABS observed in the scattering of 29-MeV α particles on ^{40}Ca was made by Thomson[31] by introducing an interaction $V_{\alpha\alpha}$ (between two α particles).

Allowance for the interaction $V_{\alpha\alpha}$ by the distorted-wave method leads to the Schrödinger equation describing $A(\alpha,\alpha)A$ elastic scattering:

$$(T_{\alpha A}+V_0)\,\varphi_{\alpha A}+\langle\varphi\,|\,V_{\alpha\alpha}\,|\,\varphi\varphi_{\alpha A}\rangle=E\varphi_{\alpha A}. \tag{23}$$

where $\varphi_{\alpha A}$ is the wave function of elastic scattering; φ is a bound-state wave function of the target nucleus. The integration is with respect to the relative internal coordinates of the core, $C=A-\alpha$, and the α cluster. The bound-state wave function of the target nucleus is taken in the form

$$\varphi=\sum_n \sqrt{S_n}\,\varphi_{Cn}\xi_{Cn}\xi_\alpha,$$

where S_n is the spectroscopic factor; ξ_{Cn} is the internal wave function of the core; φ_{Cn} is the wave function of the relative motion; and ξ_α is the wave function of the α particle. Only the relative S state is considered. The interaction $V_{\alpha\alpha}$ is taken in two forms; in the approximation of zero range of the nuclear forces, $V_{\alpha\alpha}=V_L^B\delta(\mathbf{r}_{12})$, and in the Ali-Bodmer form[32]:

$$V_{\alpha\alpha}(r_{12})=V_{\alpha R}\exp(-\mu_R^2 r_{12}^2)-V_A\exp(-\mu_A^2 r_{12}^2).$$

Earlier attempts to take into account the interaction $V_{\alpha\alpha}$ had already been made.[33] However, as Agassi and Wall show,[29] the interaction $V_{\alpha\alpha}$ estimated by Schmeing[33] does not give any peak in l space. A shortcoming of Thomson's work is the neglect of antisymmetrization and the assertion that only low partial waves are important. By and large, Thomson's explanation of ABS does not succeed.

Hitherto, none of the attempts to explain ABS by cluster-cluster interaction have had particular success. However, we regard their further development as promising, since such approaches can clarify ABS at the microscopic level.

6. OPTICAL MODEL WITH l-DEPENDENT IMAGINARY PART

In Ref. 34, a fairly successful attempt was made to reproduce backward scattering and the structure of the elastic-scattering excitation functions by the introduction of an l dependence of the imaginary part W of the potential:

$$W(r,\,l)=W_0(r)\,F(l), \tag{24}$$

where $W_0(r)$ is the ordinary form factor of the optical model; $F(l)$ is a factor which depends on the orbital angular momentum (strictly speaking, for the scattering of particles with spin l must be replaced by the total spin $J=|l+I_t+I_N|$ of the ingoing channel, but generally the model is used for spinless particles).

The function $F(l)$ is chosen in such a way as to reduce the absorption of partial waves with angular momenta near the critical l_c; usually, $F(l)$ is taken in the form

$$F(l)=\{1+\exp[(l-l_c)\,\Delta l]\}^{-1}. \tag{25}$$

Thus, particles with large l are absorbed less, so that the probability of being scattered back into the elastic channel is greater than in the ordinary optical model. Therefore, the scattering is mainly determined by high angular momenta, i.e., the main contribution to the cross section is made by a few Legendre polynomials with $l\sim l_c$:

$$\frac{d\sigma}{d\Omega}(\Theta)\sim\left|\sum_{l_c-\Delta l}^{l_c+\Delta l} a_l P_l(\cos\Theta)\right|. \tag{26}$$

Since Legendre polynomials at higher l have larger values at small and large angles, this increases the backward scattering (the growth of the forward scattering is unimportant because Rutherford scattering predominates).

The physical meaning of this procedure, which reduces the absorption of high partial waves, is that for some colliding nuclei there may be a large difference between the angular momenta in the ingoing channel and the accessible angular momenta in the outgoing channel. If the high angular momentum introduced by a grazing collision of two heavy ions, i.e., in the case when $l\sim l_c$, is to be carried away, outgoing channels with sufficient decay energy and, which is particularly important, with the emission of particles of sufficiently high mass, must be open. But if the system decays basically by the emission of a neutron, absorption in the ingoing channel will be weakened.

The experiments have revealed a connection between the character of the large-angle scattering and the number of channels of the decaying system. As an example, Fig. 19 shows the $^{12}C+^{16}O$ and $^{12}C+^{19}F$ scattering cross sections[35] and Fig. 20 the decay channels of the corresponding systems. In the $^{12}C+^{16}O$ case, appreciably fewer channels are open, and the scattering cross section exhibits strong oscillations and a growth of the cross section at large angles.

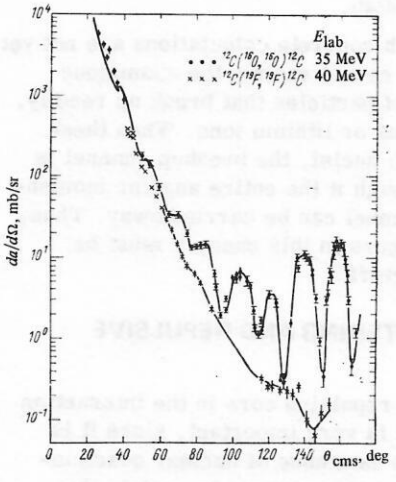

FIG. 19. Angular distributions of elastic scattering of 35-MeV ^{16}O ions and 40-MeV ^{19}F ions on ^{12}C nuclei. The continuous curves are drawn through the points.

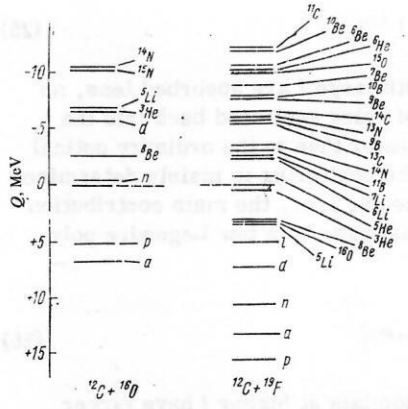

FIG. 20. Q reactions for the ground state of different channels in the $^{12}C+^{16}O$ and $^{12}C+^{19}F$ reactions.

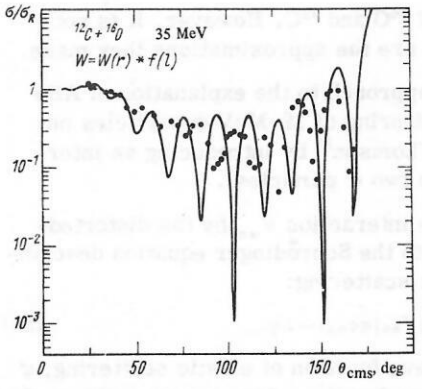

FIG. 21. Calculation of the elastic scattering of 35-MeV oxygen ions on ^{12}C nuclei in accordance with the optical model with l-dependent imaginary part of the optical potential for $V=14$ MeV, $W(r)=0.4+125E$, $R=6.25$, $a=0.45$, $l_c=9.2$.

Figure 21 shows the results of calculations in accordance with the optical model with l-dependent imaginary part for $^{12}C+^{16}O$ scattering. It can be seen that the agreement in the region of large angles is perfectly satisfactory.

A model with l-dependent imaginary part means the introduction of the two additional parameters l_c and Δl. In the calculations, attempts are made to choose these parameters on the basis of physical arguments and not arbitrarily. Thus, one takes $l_c=(2\mu/\hbar^2)^{1/2}\overline{R}(E+\overline{Q})^{1/2}$, where $\overline{R}$ and $\overline{Q}$ are the radius and the threshold of the main channel through which decay is possible. It is obvious that considerable arbitrariness is possible here.

The model with l-dependent imaginary part has made it possible to associate the appearance of weak absorption with the properties of an intermediate system and explain phenomenologically effects due to weak absorption. Actual computational successes of the model are rather sparse. It can be used to explain large-angle scattering and the structure of the excitation functions for some cases. However, difficulties arise with the description of scattering through small angles (as can also be seen from Fig. 21) and the explanation of data obtained at different energies. The additional parameters of the model in fact are free, and their total number (eight) is too high.

In addition, although concrete calculations are not yet available, this model cannot explain the anomalous backward scattering of particles that break up readily, for example, deuterons or lithium ions. When these particles interact with nuclei, the breakup channel is always open, and through it the entire angular momentum of the ingoing channel can be carried away. Thus, if weak absorption occurs in this case, it must be explained by other factors.

7. BACKWARD SCATTERING AND REPULSIVE CORE

The question of the repulsive core in the interaction of two complex nuclei is very important, since it is directly related to the existence of nuclear quasimolecules. It first arose in the attempt to explain the resonance structure in $^{12}C+^{12}C$ scattering. The interaction potential shown in Fig. 22 was proposed.[36] It was assumed that the observed resonances correspond to levels in a potential pocket, which can decay either in the exterior region, i.e., back into the elastic channel, or through the interior barrier, forming a compound nucleus which subsequently decays in the ordinary ways. In the case of the $^{12}C+^{12}C$ system, these levels in the second well are quasimolecular states.

At the present time, the literal interpretation of resonances in the energy dependence of the scattering cross section as one-particle quasimolecular states is regarded as uproven, since it is difficult to choose a potential well with sensible parameters that could contain the necessary number of levels with the correct distances between them. Nevertheless, more and more data are accumulating[25,37] which indicate that quasimolecular states in nuclei exist and that for their explanation one must invoke the notion of a repulsive core within the nucleus.

The existence of a repulsive core in the potential interaction of two complex nuclei follows from the Pauli principle, which forbids their mutual interpenetration. This question has been considered in detail on a number of occasions (see, for example, Ref. 37). Let us consider here one example—the interaction of two α particles. In this interaction a repulsive core is manifested, as a result of which quasimolecular states of the nucleus are formed.[37]

Figure 23 gives the $\alpha\alpha$ phase shifts obtained from different experiments. The phase shift δ_2 begins to increase rapidly from an energy about 1 MeV and δ_4 from an energy about 6 MeV. This indicates an extension with a fairly abrupt boundary in the exterior region with $R\leq 4$ F (the impact parameter $b=\lambda L$ is approximately 4 F at $E_{cms}=1$ MeV and ~3 F at $E_{cms}=6$ MeV).

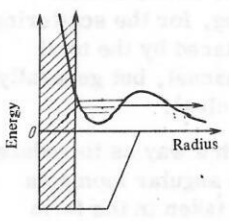

FIG. 22. Schematic interaction potential for heavy ions: The hatched region is the repulsive core; the arrows indicate the possible decay routes of quasimolecular states.

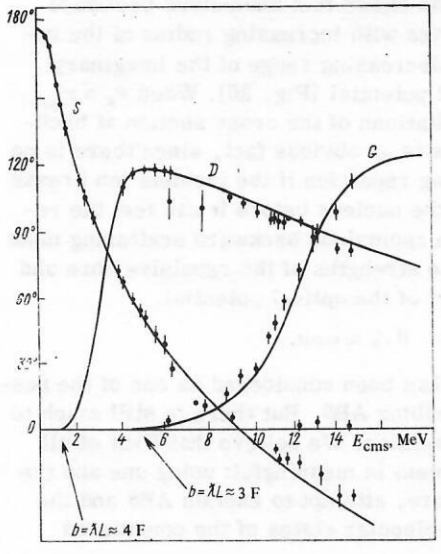

FIG. 23. Phase shift of $\alpha\alpha$ scattering obtained from phase-shift analysis of the experimental data.

The monotonic decrease of δ_0 from $E_{cms}\approx 5$ MeV, i.e. $b\approx 2$ F, and the decrease of δ_2 indicate strong internal repulsion, at least for $L=0$ and 2.

This character of the scattering can be well described by a phenomenological potential with repulsive core. The form of this potential for different L is shown in Fig. 24,[37] and the phase shifts calculated by means of it are shown in Fig. 23 by the continuous curves, which show excellent agreement with experiment.

In the chosen potential quasibound 0^+, 2^+, 4^+ levels arise and form the well-known rotational band of the ^{8}Be nucleus: 0—2.9 MeV—11.4 MeV. The levels of this band have α-particle widths approximately equal to the Wigner limit $3\hbar^2/2m_\alpha R_\alpha^2$. The distance between the levels corresponds to a moment of inertia $m_\alpha R_\alpha^2$ with $R_\alpha\approx 4.5$ F. All three levels of the band are not only manifested in $\alpha\alpha$ scattering but are also strongly excited in such reactions[25] as ^{6}Li$(\alpha,d)^8$Be and ^{7}Li$(\alpha,t)^8$Be, in which the replacement mechanism and, therefore, the formation of a ^{8}Be nucleus from two α particles are possible.

Thus, all the existing experimental data are well explained by the assumption that in the $\alpha\alpha$ system there is a potential with a repulsive core leading to the formation of quasimolecular states. There are data[38] which enable one to extend this picture to excitation energies of about 60 MeV and identify levels with $L=6$ and 8.

It is of interest to compare this nuclear quasimolecular potential with an ordinary molecular potential. Such a comparison[37] is made in Fig. 25, which shows the potential for the ground state of the hydrogen molecule and the nuclear part of the $\alpha\alpha$ potential for the ground state of the ^{8}Be nucleus (as a result of the subtraction of the Coulomb interaction, the ^{8}Be nucleus, which is in fact unstable, becomes weakly bound).

It can be seen that the two potentials have much in common, although the nuclear quasimolecular potential is approximately 40 times weaker (in units of $\hbar^2/M_0R_c^2$,

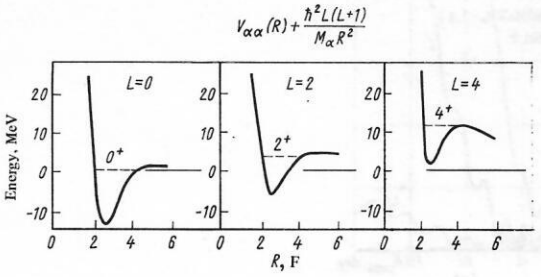

FIG. 24. Potentials of $\alpha\alpha$ scattering used to calculate the phase shifts shown in Fig. 23; the dashed lines are the quasi-bound states of ^{8}Be: 0^+, 2^+, 4^+.

where M_0 is the mass of the subsystem and R_c the radius of the core) than the ordinary molecular potential. As a result, the localization of the "nuclear atoms" is much less definite. Because of this, the distinction between vibrational and rotational degrees of freedom is much less rigorous in the case of a nuclear quasimolecule.

The work of Japanese theoreticians (see, for example, the review Ref. 37) shows that a phenomenological $\alpha\alpha$ potential with repulsive core can be obtained microscopically as a result of the Pauli principle. At the same time, the connection to the ordinary shell model is not lost. The repulsive core at a radius of approximately 2 F arises as a node of the wave function, which oscillates in the internal region and rapidly increases in amplitude in the exterior region (for $R>2$ F).

Baz' and Zhukov,[39] using the method of K harmonics and taking into account the Pauli principle, conclude that there is a repulsive core for collision of nuclei. Baz'[40] estimates the size of the repulsive core, which turns out to be rather wide:

$$(r)_{\text{core}}=(R_1+R_2)\left[1-\frac{A}{A_1A_2}\cdot\frac{\rho_0^3}{(R_1+R_2)^2}\cdot\frac{1}{\Gamma}\ln\Gamma\right]\approx(R_1+R_2), \quad (27)$$

where R_1 and R_2 are the radii of the colliding nuclei; A_1 and A_2 are the mass numbers; ρ_0 is the variable in the method of K harmonics; and Γ is a number related to ρ_0.

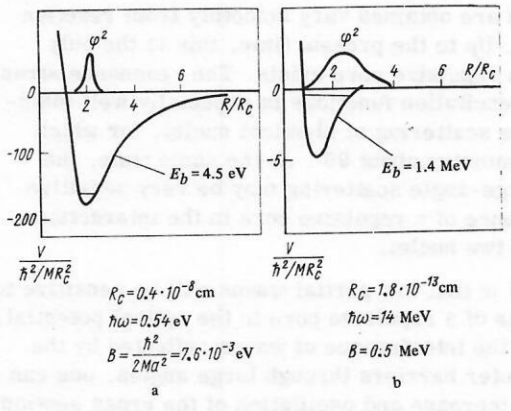

FIG. 25. Comparison of potentials for the ground states of the hydrogen molecule (a) and the "nuclear molecule" ^{8}Be (b). In the case of ^{8}Be only the nuclear part of the potential is given. The relative distances are given in units of the radius R_c of the repulsive core, the energy in units of $\hbar^2/\mu R_c^2$.

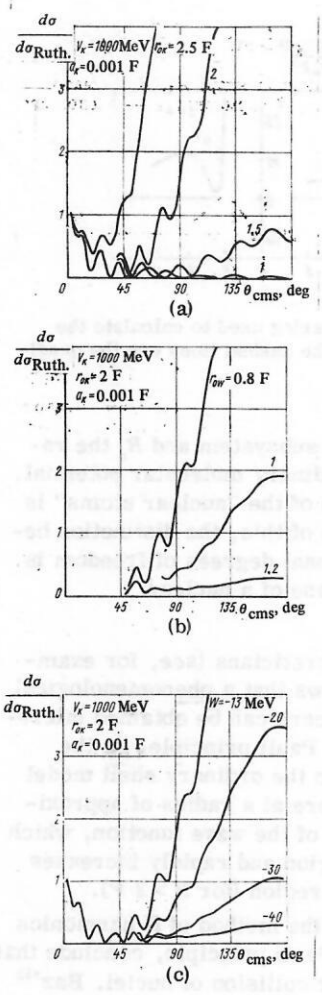

FIG. 26. Optical model with repulsive core in the case of elastic scattering of α-particles on ^{12}C nuclei; b) influence of the radius of the imaginary part of the optical potential on the ABS; c) influence of the magnitude of the imaginary part of the optical potential on the ABS.

Many attempts have been made to detect a repulsive core in the scattering of more complicated nuclear systems. In particular, by adding an optical potential to the core, Michaud[41] attempts to explain the structure of the excitation functions.

It turns out that if one fits simultaneously the three reactions $^{12}C+^{12}C$, $^{16}O+^{16}O$, and $^{12}C+^{16}O$, agreement between the calculations and experiment can be achieved only if there is a repulsive core; moreover, the parameters which are obtained vary smoothly from reaction to reaction. Up to the present time, this is the only proof that a repulsive core exists. The resonance structure of the excitation functions is especially well manifested in the scattering of identical nuclei, for which there is symmetry about 90°. At the same time, the study of large-angle scattering may be very sensitive to the presence of a repulsive core in the interaction potential of two nuclei.

The point is that low partial waves will be sensitive to the presence of a repulsive core in the optical potential. Because of the interference of waves reflected by the inner and outer barriers through large angles, one can observe an increase and oscillation of the cross sections (Newton's rings are an analogous phenomenon in optics). To understand the role of a repulsive core in scattering, repulsion in the form of a hard core was introduced into the optical potential.

The investigation shows that anomalous backward scattering increases with increasing radius of the repulsive core and decreasing range of the imaginary part of the optical potential (Fig. 26). When $r_W > r_{core}$, there are no oscillations of the cross section at backward angles. This is an obvious fact, since there is no point in introducing repulsion if the incident ion breaks up in the field of the nucleus before it can feel the repulsive core. The anomalous backward scattering must be governed by the strengths of the repulsive core and the imaginary part of the optical potential:

$$V_{core}\, r_{core}^2 \approx \text{const}; \quad W r_W^2 \approx \text{const}.$$

A repulsive core has been considered as one of the possible ways of decribing ABS. But there is still much to be done in this direction. We believe that first of all the following problem is meaningful: using one and the same repulsive core, attempt to explain ABS and the spectra of quasimolecular states of the considered nuclei.

8. DESCRIPTION OF BACKWARD SCATTERING BY MEANS OF REGGE POLES

One of the most modern and most successful methods of describing ABS is the Regge-pole method developed by Cowley and Heymann[42] and most consistently by McVoy.[43] The idea of the Regge method is that the angular momentum l is regarded as a variable capable of taking any complex values. As before, physical meaning attaches to positive integral (in units of $\hbar$ or $\hbar/2$) values of the angular momentum.

With each bound or resonant state a pole of the S matrix is associated. With varying energy, this pole is displaced in the complex l plane. This is the trajectory of the Regge pole. These trajectories are used to classify bound and resonant states in nonrelativistic quantum mechanics and elementary particles and resonances in the theory of elementary particles. On one trajectory there may be a group of bound states with different l but the same principal or radial quantum number.

The introduction of a pole term in the $S(l)$ matrix is

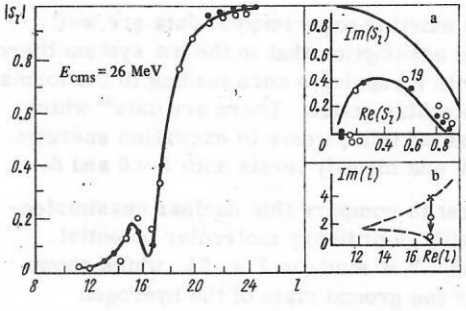

FIG. 27. Dependence of the modulus $|S_l|$ of the S-matrix element or the reflection coefficient on the angular momentum l: a) Argand diagram for $l = 14-22$; b) positions of the pole (*) and zero (0) on the complex l plane; ●●● analysis of scattering of ^{16}O ions on ^{16}O nuclei by the diffraction model with sharp edge with one Regge pole; ○○○ parameters of model obtained by fitting to the angular distribution in the framework of the optical model.

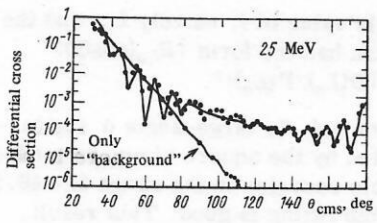

FIG. 28. Angular distribution corresponding to Fig. 27: the oscillating curve is a model six-parameter fit; the decreasing curve is the background. ABS is due to a Regge pole.

a convenient way of describing, for example, a rotational band of quasimolecular states.

According to McVoy,[43] the $S(l)$ matrix for given energy can be represented in the form

$$S(l) = B(l)\left[\frac{l-L_0-iz(l)}{l-L_0-ip(l)}\right] = B(l)\left[1+i\frac{D(l)}{l-L_0-i\Gamma(l)/2}\right], \qquad (28)$$

where $B(l)$ describes the background nonresonant scattering and can be calculated by the diffraction or the optical model. Part of the Breit-Wigner S matrix describes resonance in l space with elastic width $D(l)$ and total width $\Gamma(l)$ and with center at angular momentum L. In the rigid rotator model, the angular momentum L is the angular momentum of the rotator. For convenience, McVoy assumes the following form for $D(l)$ and $\Gamma(l)$:

$$D(l) = D[1+\exp(l-L)/\Delta]; \quad \Gamma(l) = \Gamma[1+\exp(l-L)/\Delta]. \qquad (29)$$

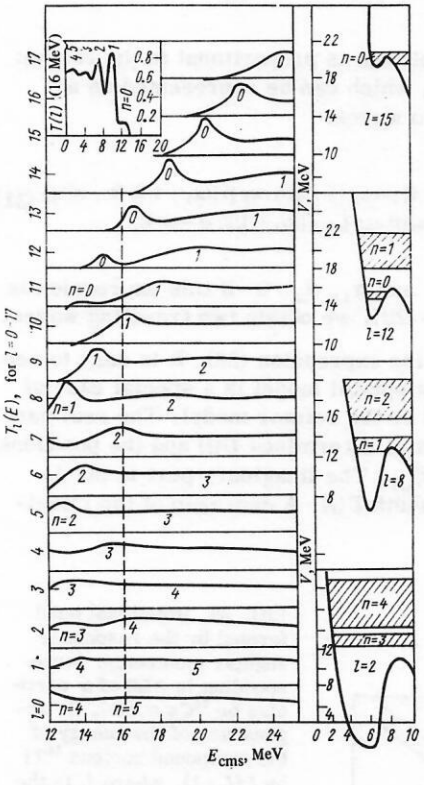

FIG. 29. Dependence of the optical-model T_l for $l=0$—17 on E_{cms}. The maxima correspond to the quantum numbers n: a) dependence of T_l on the angular momentum l for $E_{cms}=16$ MeV; b) behavior of resonances in the potential pocket—$V(r)+V_{Coul}+\hbar^2 l(l+1)/(2\mu r^2)$.

Here, Γ and D play the role of reduced widths. Obviously, $z(l)$ and $p(l)$ have the same dependence as Eq. (29). The reduced pole p and the reduced zero z are defined as follows: $p=\Gamma/2$ and $z=\Gamma/2-D$. In this formalism, L_0, Γ, and D are the parameters of the Regge resonance. The $S(l)$ matrix has a pole at $l\approx L_0+ip(L_0)$, and a zero at $l\approx L_0+iz(L_0)$. There will always be a pole in the upper l half-plane and a zero in the lower half-plane if $D>\Gamma/2$. Figure 27 shows the modulus of the S-matrix element describing the scattering of ^{16}O ions on ^{16}O nuclei at $E_{^{16}O}=26$ MeV. The parameters of the model are: $\Gamma=6.04$, $D=2.76$, $L_0=17.2$, $L=17.3$, and $\Delta=1.4$. Here, only one Regge pole is taken into account.

The corresponding angular distribution of elastically scattered oxygen ions is shown in Fig. 28, which shows that the one-pole Regge approximation ensures an oscillating structure at backward angles.

We define the $S(l)$ matrix as a function of the complex energy E and angular momentum l. Then a pole will be found at a definite combination of l and E in the case of a bound state and near it in the case of resonance. Poles can be observed most clearly as resonances in the l-dependence of the transmission coefficient $T(l,E)=1-|S(l,E)|^2$ at fixed energy $E_{n,l}$. These resonances appear with increasing energy $E_{n,l}$ with corresponding increase of the radial energy (the principal quantum number n corresponds to it) and rotational energy (to which the orbital angular momentum l corresponds). The corresponding transmission coefficients T_l as functions of the energy will exhibit potential resonances and their echoes, and the potential curves $[-V(r)+V_{Coul}+\hbar^2 l(l+1)/(2\mu r^2)]$ for a given angular momentum l will demonstrate filling of the potential pocket by corresponding n-states. This situation is well demonstrated by Fig. 29, taken from Ref. 43. It shows that some resonances move faster than the height of the barrier, are mani-

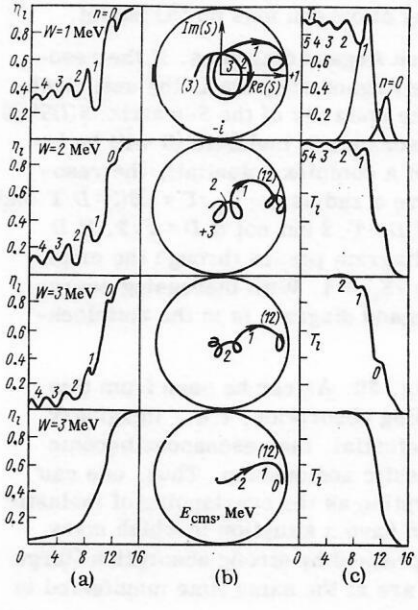

FIG. 30. Strong absorption as a result of overlapping of Regge resonances: a) reflection coefficient as a function of the angular momentum for different imaginary parts of the optical potential; b) Argand diagrams; c) transmission coefficients.

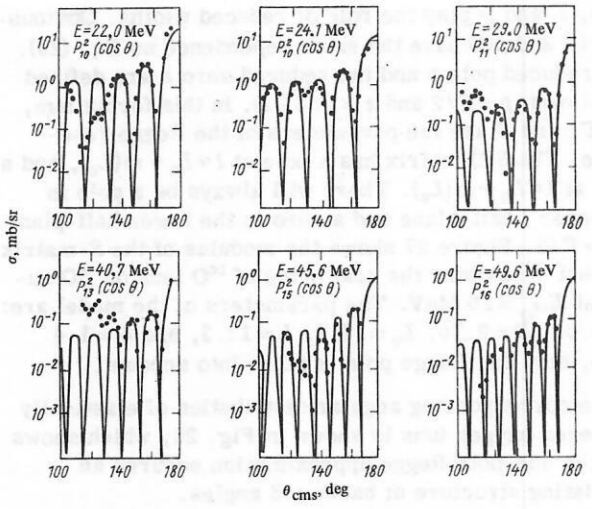

FIG. 31. Fitting of the ABS of α particles on ^{40}Ca nuclei by the square of one Legendre polynomial $P_l(\cos\Theta)$.

fested several MeV higher than the barrier, broaden, and disappear into the background. The energy at which resonances no longer exist will be called the filling energy. As can be seen from the expression (28) and Fig. 29, as E and l move along the Regge trajectory the resonances are raised above the barrier and increase their elastic width to $D=\Gamma/2$ and accordingly $T=1$. For small l and E, we have $D<\Gamma/2$ and a resonance is basically inelastic, whereas $D>\Gamma/2$ for large l and E and elastic resonance occurs.

As we have already pointed out, absorption in the framework of the optical model can be interpreted as due to completely overlapping Regge resonances. This can be seen best in Fig. 30, which shows the moduli of the S-matrix elements and the transmission coefficients for different l (the radial quantum numbers n show the position of the resonance) and also the Argand diagrams for elastic scattering of oxygen ions on ^{16}O nuclei.

Now a few words on Argand diagrams. If the resonance is elastic, the Argand diagram is the unit circle. This follows from the unitarity of the S-matrix: $S(l)S^*(l)=1$. If the Regge resonance is inelastic (it will be inelastic in the case of a complex potential), the resonance circle will have a radius $\rho=\Gamma_{el}/\Gamma\approx|B(l)|D/\Gamma$ and enclose the origin if $D>\Gamma/2$ but not if $D<\Gamma/2$. If $D=\Gamma/2$, the Argand diagram passes through the origin. This corresponds to $|S_l|=1$. With increasing energy, the motion in the Argand diagram is in the anticlockwise sense.

We now turn to Fig. 30. As can be seen from this figure, with increasing absorption, i.e., imaginary part of the optical potential, the resonances become more and more inelastic and overlap. Thus, one can regard strong absorption as the overlapping of inelastic resonances. One can have a situation in which many resonances are suppressed by strong absorption (large imaginary part) but are at the same time manifested in the excitation functions.

Let us consider again the expression (28). If $\Gamma(l)$ is not greater than one unit of $\hbar$, the resonance amplitude is determined by a single value of l, namely L_0, and the large-angle cross section has the form $|R_{L_0}(\cos\Theta)|^2$ with weight coefficient $|D(L_0)/\Gamma(L_0)|^2$.

In Fig. 31, taken from Ref. 7, large-angle α scattering on ^{40}Ca nuclei is fitted by the square of one Legendre polynomial for α-particle energies in the range 22—49.5 MeV. At all energies, the fitting is good. This result, obtained for only one angular momentum, or when one Regge pole contributes to the scattering, and for which good agreement between theory and experiment is observed, indicates that there is a resonance of the form corresponding to a quasimolecular state.

Figure 32, taken from Ref. 7, shows the energy of the ^{44}Ti compound nucleus as a function of the resonance angular momentum describing the anomalous backward scattering of α particles on the ^{40}Ca nucleus (dashed curve) and as a function of the orbital angular momentum corresponding to a grazing collision ($|S_l|\sim 1/2$) (continuous curve). These two curves should coincide. The discrepancy may be due to the excitation of the core or to the rotational band beginning with a nonzero principal quantum number.

According to Fuller,[44] quasimolecular resonance can be regarded as a decaying surface wave propagating around the region of strong absorption. We use the Szegö asymptotic representation for Legendre polynomials:

$$P_\alpha(\cos\Theta) = \frac{\Gamma(\alpha+1)}{\Gamma(\alpha+3/2)}\left(\frac{\pi}{2\sin\Theta}\right)^{1/2}\cos\left[(\alpha+1/2)\Theta-\frac{\pi}{4}\right];\ \sin\Theta\geqslant 1/|\alpha|. \tag{30}$$

The scattering amplitude is proportional to the cosine: $\cos[(\alpha+\frac{1}{2})\Theta-\pi/4]$, which can be represented as a superposition of two waves:

$$\begin{aligned}\cos[(\alpha+1/2)\Theta-\pi/4] &= \exp(-\alpha_2\Theta)\exp\{i[(\alpha_1+1/2)\Theta-\pi/4]\}\\ &+\exp(\alpha_2\Theta)\exp\{-i[(\alpha_1+1/2)\Theta-\pi/4]\},\end{aligned} \tag{31}$$

where $\alpha=\alpha_1+i\alpha_2$, and α_1, $\alpha_2>0$. If this expression is multiplied by $\exp(-iEt)$, we obtain two traveling waves.

Let us return to the expression (28). It is easy to see that the l-dependent optical model is a special case of the expression (28) or the rotator model. The real part of the optical potential determines $D(l)$ and the positions of the resonances $E_{n,l}$. The imaginary part is manifested in the total width $\Gamma(l)$. A decrease of the imagi-

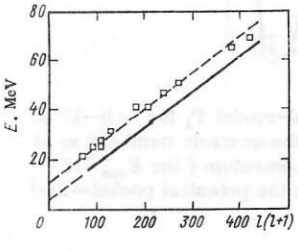

FIG. 32. Rotational band formed by the resonance angular momentum corresponding to ABS of α particles on ^{40}Ca nuclei. □: dependence of the energy of the compound nucleus ^{44}Ti on $L(L+1)$, where L is the resonance angular momentum ($l=L_{res}$); —: $l_0(l+1)$, where l_0 is the angular momentum of a grazing collision, $l=kR$.

nary part of the optical potential for partial waves near L_0 presupposes that $\Gamma(L_0)$ is small. This leads to anomalous scattering if $D(l)$ is not small, and then $\Gamma(l)$ and not $D(l)$ is determined by the structure of the target nucleus. To explain the isotopic effect in the anomalous backward scattering of particles on Ca isotopes, we shall assume that $D(l)$ is proportional to the α reduced width of the resonance; then a small value of $D(l)$ will be associated with the disappearance of ABS. In some cases,[45] the one-pole approximation is inadequate, and then two or more Regge poles are introduced. Although the agreement with experiment can then be improved, the physical clarity of the picture is to some extent lost.

The successes of the Regge-pole method in the description of anomalous backward scattering are particularly valuable because this method establishes a direct relation between elastic scattering and highly excited states of spherical structure, which are hard or impossible to identify otherwise.

CONCLUSIONS

Until recently, it appeared that the study of scattering had become largely obsolete. The data being obtained had the character of refinements of something already known, and discussion concentrated on the details of particular models. In addition, the models were sometimes unnecessarily complicated but without qualitatively new physical phenomena, and comparison between experiments and calculations sometimes reduced to the fitting of parameters.

The discovery of anomalous backward scattering showed that the simplest process in nuclear dynamics—elastic scattering—is much richer in its manifestations than had been assumed from the point of view of existing models. The most interesting thing is that ABS was found to be intimately related to features of nuclear structure that can only be studied with difficulty and sometimes not at all by other methods. Thus, anomalous backward scattering, originally a vexing flaw in the elegance of the optical-model concepts of scattering, was transformed into a serious instrument for investigating nuclear structure.

There is no unified description of ABS, nor can there be. Some of the effects are due to the existence of clusters in the ground states of the colliding nuclei (exchange, scattering on clusters); others are due to the formation of a resonance cluster of the intermediate system at high excitations. It is possible that in some cases there is no direct connection between ABS and quasimolecular structure. The only common feature is that to explain ABS one must dispense with the concept of strong absorption in the surface layer of the nucleus.

In the cases when the energies of the incident particles are near the Coulomb barrier and the colliding nuclei have similar structures, exchange models are best in the description of ABS; however, when resonances are not observed in the excitation functions but ABS occurs, the Regge-pole model is preferable. In the cases when there are isolated resonances at large angles in the excitation functions, one can use the simplest models, in particular, an optical model with resonant phase shifts or an optical model with l-dependent imaginary part.

If isolated resonances at large angles are present in the excitation functions and it is assumed that the main contribution to the large-angle cross section is not made by potential scattering, one can relate anomalous backward scattering and the cluster transfer reaction to the excitation of quasibound states whose widths are near the Wigner limit. The large-angle cross section at resonance is proportional to the spectroscopic factor of the quasibound state. Models which treat scattering on substructures require further development. A model with a repulsive core is particularly attractive. In the light of the most recent work of the Japanese theoreticians,[37] the repulsive core is associated with the Pauli principle, or, putting it more precisely, with its new role—the formation of a phase of molecular matter. Another interesting problem in the study of ABS is the measurement of excitation functions on the time scale. The oscillations in the excitation functions have a quantum character, as in the case of atomic collisions.

Although many features of ABS are already understood, many unresolved questions remain. To a large extent this is due to the serious shortage of experimental data. It is not clear, for example, whether ABS is manifested on nuclei heavier than the calcium nuclei. There are very few ABS data for ^{3}He nuclei, which have properties closest to those of α particles. The ABS of weakly bound nuclei like ^{6}Li remains unexplained. One can be sure that in the coming years both the theoretical and experimental study of anomalous backward scattering will remain among the most interesting problems of nuclear physics.

[1]A. Donnachie, Rep. Progr. Phys. **36**, 695 (1973).
[2]U.C. Voos, W. Von Oertzen, and R. Bock, Nucl. Phys. A **135**, 207 (1969).
[3]J. V. Maher *et al.*, Phys. Rev. **188**, 1665 (1969).
[4]C. Bergman and R.K. Hobbie, Phys. Rev. C **3**, 1729 (1971); M.K. Mehta, W.E. Hunt, and R.H. Davis, Phys. Rev. **160**, 791 (1967); A. Budzanowski and K. Grotowski, Phys. Lett. **16**, 135 (1965); H.I. Kim, Phys. Lett. **19**, 296 (1965); J.R. Rook, Nucl. Phys. A **142**, 113 (1970); H. Oeschler *et al.*, Phys. Rev. Lett. **28**, 694 (1972); R.H. Davis, 5th Summer School on Nuclear Physics 20.08—3.09, Rudziska, Poland (1972), Report P-N 1447/1/PL/C, Warsaw, 1973, p. 122. Gaul *et al.*, Nucl. Phys. **137**, 177 (1969); B.I. Kuznetsov *et al.*, Yad. Fiz. **18**, 950 (1974) [Sov. J. Nucl. Phys. **18**, 490 (1974)].
[5]H. Fuchsi, Max-Planck-Institute Kernphysik, Jahresbericht, Heidelberg, 1970, p. 26.
[6]V.I. Chuev *et al.*, J. Phys. (Paris), Colloq., No. 6, 161 (1971).
[7]R. Stock *et al.*, Phys. Rev. C **6**, 1226 (1972).
[8]C.R. Gruhn and N.S. Wall, Nucl. Phys. **81**, 161 (1966).
[9]I.A. Gubkin, Yad. Fiz. **11**, 598 (1970) [Sov. J. Nucl. Phys. **11**, 336 (1970)].
[10]K.W. Ford and J.A. Wheeler, Ann. Phys. **7**, 259 (1959).
[11]H.C. Bryant and N. Jarmie, Ann. Phys. **47**, 127 (1968).
[12]Van de Hulst, Rasseyanie Sveta Malymi Chastitsami [Russian translation from German, Light Scattering by Small Particles], Izd-vo Inostr. Lit. Moscow (1961).
[13]A. Bobrowska *et al.*, Nucl. Phys. A **126**, 361 (1969).
[14]A. Budzanowski *et al.*, Nucl. Phys. A **126**, 369 (1969).
[15]R. Davis, Symposium on Recent Progress in Nuclear Physics with Tandems, Heidelberg, Germany, July (1966).

[16]E. B. Carter *et al.*, Phys. Rev. **133**, B1421 (1964).
[17]G. M. Temmer, Phys. Lett. **1**, 10 (1962).
[18]W. Von Oertzen, Nucl. Phys. A **148**, 529 (1970).
[19]W. Von Oertzen, in: International Conference on the Physics of Heavy Ions, Dubna, February 11—17, 1971 [in Russian], Dubna, 1971, p. 350.
[20]G. Baur and C. K. Gelbke, Nucl. Phys. A **204**, 138 (1973).
[21]H. Rosenthal and H. M. Foley, Phys. Rev. Lett. **23**, 1480 (1969).
[22]H. Kelleter *et al.*, Nucl. Phys. A **210**, 502 (1973).
[23]S. V. Bobashev, in: Proc. Intern. Conf. on the Physics of Electronic and Atomic Collisions, Amsterdam, 26—30 July 1971 (Ed. T. R. Govers and F. J. de Heer), North Holland, Amsterdam, 1972, p. 38.
[24]S. V. Bobashov, ZhÉTF Pis'ma Red. **11**, 389 (1970) [JETP Letters **11**, 260 (1970).
[25]A. A. Ogloblin, Fiz. El. Chast. Atom. Yad. **3**, No. 4, 936 (1972) [Sov. J. Part. Nucl. **3**, 467 (1973)].
[26]V. I. Chuev *et al.*, J. Phys. (Paris), Colloq., No. 6, 163 (1971).
[27]D. Bachelier *et al.*, Nucl. Phys. A **195**, 361 (1972).
[28]I. V. Kurdyumov *et al.*, Phys. Lett. B **31**, 426 (1970).
[29]D. Agassi and N. S. Wall, Phys. Rev. C **7**, 1368 (1973).
[30]J. Noble and H. Coelho, Phys. Rev. C **3**, 1840 (1971).
[31]W. J. Thompson, Particles and Nuclei **2**, 47 (1971).
[32]S. Ali and A. R. Bodmer, Nucl. Phys. **80**, 99 (1966).
[33]N. C. Schmeing, Nucl. Phys. A **142**, 449 (1970).
[34]R. A. Chatwin *et al.*, Phys. Rev. C **1**, 795 (1970).
[35]R. H. Siemssen, Nuclear Spectroscopy II, Ed. by J. Cerny, Academic Press, New York (1974).
[36]D. A. Bromley *et al.*, Phys. Rev. **123**, 878 (1961).
[37]K. Ikeda *et al.*, Progr. Theor. Phys., Suppl., No. 52, 1 (1972).
[38]P. Darriulat *et al.*, Phys. Rev. B **137**, 315 (1965).
[39]A. I. Baz' and M. V. Zhukov, Yad. Fiz. **16**, 60, 958 (1973) [Sov. J. Nucl. Phys. **16**, 31, 529 (1973)].
[40]A. I. Baz', ZhÉTF Pis'ma Red. **14** (1971), p. 607 [JETP Letters **14**, 423 (1971).
[41]G. Michaud, Phys. Rev. C **8**, 525 (1973).
[42]A. A. Cowley and G. Heymann, Phys. Lett. B **30**, 618 (1969).
[43]K. W. McVoy, Phys. Rev. C **3**, 1104 (1971).
[44]R. C. Fuller, Nucl. Phys. A **216**, 199 (1973).
[45]R. Ceuleneer and F. Michel, Phys. Lett. B **43**, 365 (1973).

Translated by Julian B. Barbour